Available online at www.sciencedirect.com
SCIENCE DIRECT
International Journal of Mass Spectrometry 252 (2006) 145–150
International Journal of Mass Spectrometry
www.elsevier.com/locate/ijms

Mass spectrometric stability study of binary MS_n clusters (S = Si, Ge, Sn, Pb, and M = Cr, Mn, Cu, Zn)

S. Neukermans, X. Wang, N. Veldeman, E. Janssens, R.E. Silverans, P. Lievens *

Laboratorium voor Vaste-Stoffysica en Magnetisme, K.U.Leuven, Celestijnenlaan 200 D, B-3001 Leuven, Belgium

Received 17 November 2005; received in revised form 20 December 2005; accepted 20 December 2005
Available online 27 March 2006

Abstract

In this paper, we present a mass spectrometric stability investigation of a series of metal doped group IVA (semi-) metal clusters. Binary metal (M) doped semi-metal (S) MS_n (S = Si, Ge, Sn, Pb, and M = Cr, Mn, Cu, Zn) clusters are produced using a dual-target, dual-laser vaporization source and mass analyzed using a reflectron time-of-flight mass spectrometer. The resulting abundance spectra reveal host and dopant dependent stability information for the different systems investigated. From a comparison between the experimental abundance information and computational studies available in literature, the enhanced abundance of several sizes is interpreted in terms of peculiarly stable dopant-encapsulated cagelike structures.

Keywords: Metal clusters; Dopant; Photoionization

1. Introduction

Transition metal doped silicon and other group IVA metal clusters are extensively studied in view of the possible tuning effect of the dopant atoms on the opto-electronic, magnetic or stability properties of the host (Si_n, Ge_n, Sn_n, ...) clusters. Nearly 20 years ago, Beck, interested in the molecular level mechanism of the reaction between a metal and a semiconductor because of its technological importance, discovered stable silicon cluster–metal atom compounds of remarkable but identical stoichiometries for three different transition metal dopants, namely chromium, molybdenum, and tungsten: MSi_{15} and MSi_{16} (M = Cr, Mo, W) [1]. However, despite a valuable attempt based on a topological model [2], the magic behaviour of these structures remained unexplained for more than a decade until Kumar and Kawazoe computationally attributed the strong stability to dopant-encapsulated cage-like structures with large values of binding energy, highest occupied–lowest unoccupied molecular orbital (HOMO–LUMO) gap, and embedding energy of the dopant atom [3]. The magnetic moment of the dopants is completely quenched. An interesting property of these metal-encapsulated silicon clusters lies in the tunability of the band gap depending on the dopant M. Metal dopants can enhance the symmetry (and related geometric stability) of the host cluster or enhance the HOMO–LUMO gap into the visible region.

The initial interest in doped silicon systems [4–19], triggered by its wide use in microelectronics industry, rapidly extended to its higher mass congeners [20–25]. Notable examples, computationally predicted, are metal-encapsulated icosahedral superatoms of germanium and tin, $ZnGe_{12}$ and $CdSn_{12}$, with large HOMO–LUMO gaps or $MnGe_{12}$ and $MnSn_{12}$, with high ($5\mu_B$) magnetic moments. For doped lead clusters, besides calculational results, experimental confirmations of exceptional stabilities exist for $AlPb_{10,12}^+$, $CoPb_{10,12}^-$, $PtPb_{12}^{2-}$, and $NiPb_{10}^{2-}$ [26–29]. Besides the above mentioned observations for doped lead systems, the experimental information on metal doped group IVA clusters is mainly limited to doped silicon clusters [1,30–35] and is relatively scarce compared to the numerous computational studies existing in literature. For example, most recently, Nakajima and coworkers [35] reported the selective formation of highly stable MSi_{16} (M = Sc, Ti, V) clusters by fine tuning the laser vaporization source conditions, similar to the initial finding of C_{60} [36].

In this paper, we present a mass spectrometric stability investigation of Cr, Mn, Cu, and Zn doped Si_n, Ge_n, Sn_n, and Pb_n clusters. Electronically, Cr and Mn are characterized by a half-filled $3d^5$ shell combined with a $4s^1$ and $4s^2$ valence shell, respectively. Cu and Zn, on the other hand, have a filled $3d^{10}$ shell combined

* Corresponding author.
E-mail address: peter.lievens@fys.kuleuven.be (P. Lievens).

1387-3806/$ – see front matter © 2006 Elsevier B.V. All rights reserved.
doi:10.1016/j.ijms.2005.12.056

with a $4s^1$ and $4s^2$ valence shell, respectively. Since the stabilization of dopant-encapsulated Si_n and Ge_n cages was recently (computationally) demonstrated to be strongly guided by d-band filling of the encapsulated transition metal atom [24,37], dopants were chosen with the same 4s valence character but with a half-filled and filled 3d shell, respectively. The unoccupied 3d orbitals can accommodate (dangling bond) electrons form the Si_n and Ge_n cages, providing a strong interaction between the dopant and the surrounding cage. Moreover, all of the selected metal dopants were previously considered as dopant atoms in computational studies of metal doped group IV clusters.

2. Experiment

Binary MS_m (M = Cr, Mn, Cu, Zn, and S = Si, Ge, Sn, Pb) clusters are produced using a dual-target, dual-laser vaporization source, described in detail elsewhere [38], and mass analyzed using a reflectron time-of-flight (RTOF) mass spectrometer ($m/\Delta m = \pm 500$). The abundance of the positively charged clusters can be directly probed by the RTOF mass spectrometer (in the Wiley–McLaren configuration), whereas the neutral clusters are first laser ionized by a low fluence ArF (6.4 eV photon energy) or an F_2 (7.9 eV photon energy) excimer laser. Since we are aiming to evaluate the special stability of certain cluster sizes, it is important to mention that, in general, the mass distribution of clusters produced in a laser vaporization source does not reflect thermodynamic stabilities. Due to the low temperature of the inert gas, cluster production primarily proceeds through successive single atom addition, and the reverse process (evaporation) is often negligible. However, the cluster distribution is determined by the parameters of the source such as the metal–vapour density and dimensions of the various components of the source. Under suitable source conditions, enhanced stabilities of certain cluster species are nevertheless elucidated by enhanced abundances in mass spectra of clusters produced in a laser vaporization source. This can, for example, be reached by a sufficiently long residence time in the formation channel, allowing equilibrium between growth and evaporation, before the clusters are frozen in the adiabatic expansion. Probably, the most famous example is the discovery of C_{60}, by Smalley and coworkers, produced by laser vaporization of a graphite sheet [36]. On the other hand, the stability of positively charged clusters can be studied using high fluence laser irradiation of a beam of neutral clusters. The latter are ionized by multi-photon absorption, which, in general, causes fragmentation of metal and silicon clusters. The evaporation chain preferably stops at more stable sizes (high binding energy per atom). As a result, after photofragmentation, more stable cluster cations will be observed more abundantly.

The mass spectra for the different systems under investigation are shown in Figs. 1–5 and will be discussed in the next section. Hereby, it should be noted in advance that the cluster production was focussed on the optimization of the production of singly doped clusters for the 16 combinations studied and not all spectra shown are recorded under the same conditions of laser irradiation. In the figures, a selection of representative mass spectra is presented for which both the applied photon energy (either 6.4 or 7.9 eV) and laser fluence are indicated in the captions.

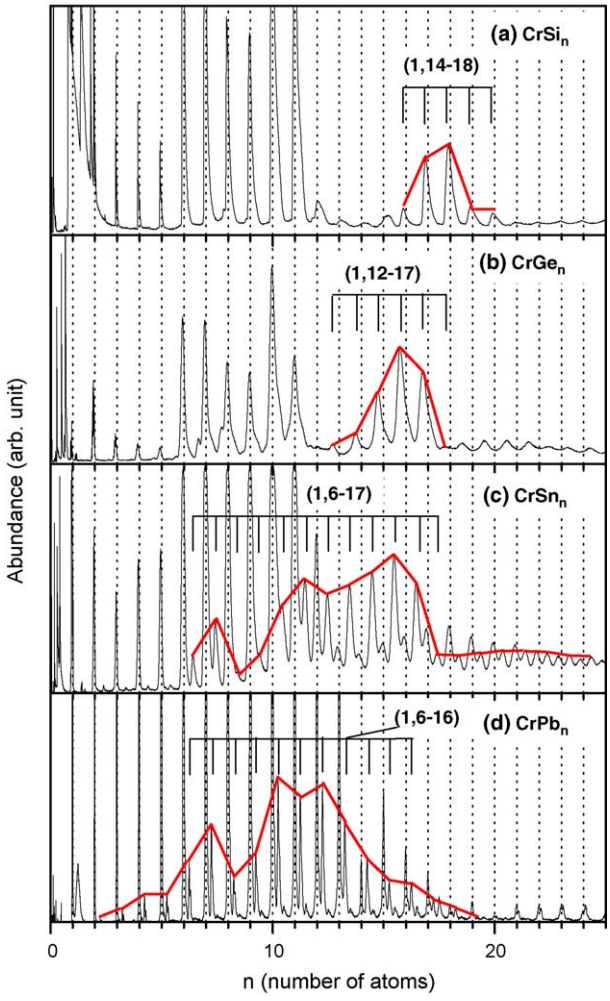

Fig. 1. Mass abundance spectra of Cr doped clusters after 6.4 eV laser ionization. Cr doped (a) Si_n (900 μJ/cm^2), (b) Ge_n (830 μJ/cm^2), (c) Sn_n (520 μJ/cm^2), and (d) Pb_n (400 μJ/cm^2).

As outlined above, depending on the applied laser fluence, the abundance spectra reflect the abundance of either cations (after multi-photon ionization and/or fragmentation) or neutral clusters (after single-photon ionization). For a low ionization laser fluence (typically <0.1 mJ/cm^2) and a photon energy sufficiently above the ionization energy of the studied species (e.g., 7.9 eV), the resulting mass spectrum reflects the distribution of the neutral species and fragmentation is negligible. Clusters investigated in this regime are symbolically denoted below as MS_n, i.e., neutral species. For sufficiently high laser fluences (typically >0.5 mJ/cm^2), the abundance spectra reflect the distribution and stability of cations after multi-photon absorption and fragmentation (notation MS_n^+). In a plot of the ion intensity versus ionizing laser fluence, both regimes can be identified. While fragmentation can result in complicated laser power dependencies due to production as well as depletion, a linear dependence at low ionizing laser intensity which intercepts the origin at zero laser power provides strong evidence for single photon ionization [30]. However, several spectra have been recorded in the

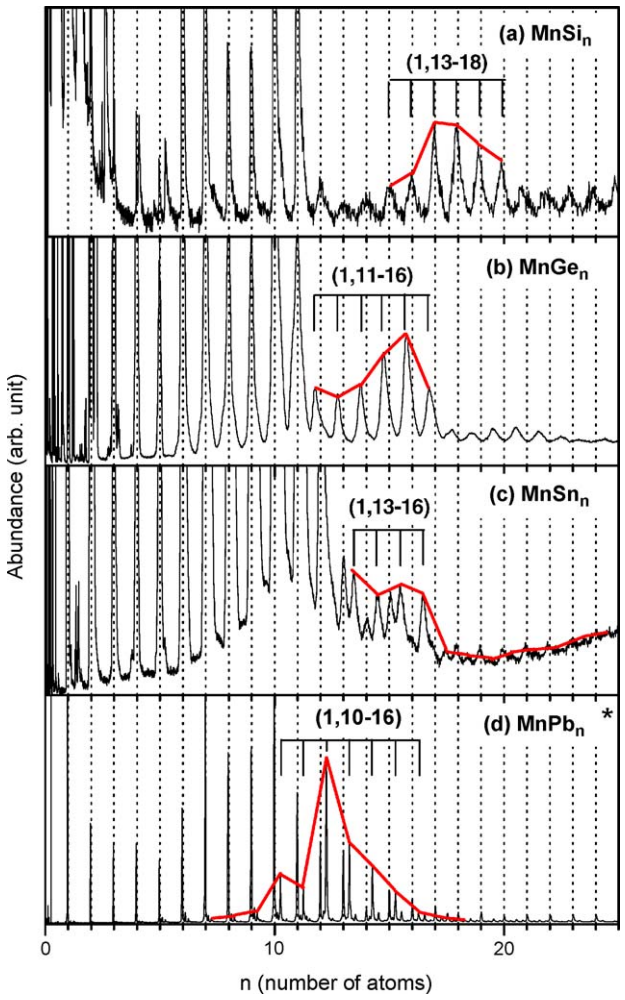

Fig. 2. Mass abundance spectra of Mn doped clusters photoionized by 6.4 eV laser irradiation for Mn doped: (a) Si_n (400 μJ/cm^2), (b) Ge_n (500 μJ/cm^2), (c) Sn_n (390 μJ/cm^2) clusters and (*) photoionized by 7.9 eV laser light for Mn doped (d) Pb_n clusters (455 μJ/cm^2).

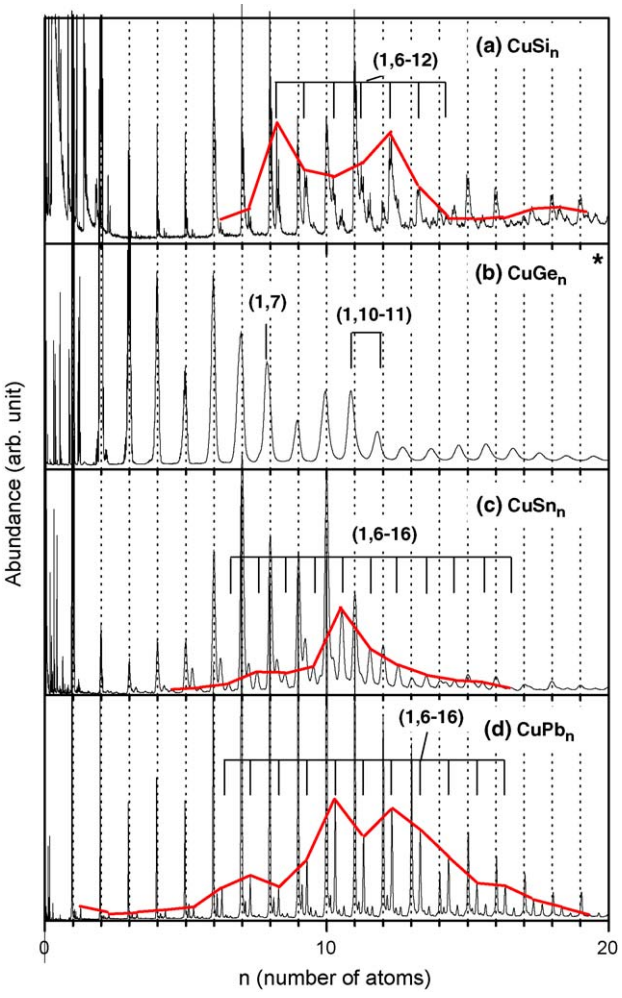

Fig. 4. Mass abundance spectra of Cu doped clusters photoionized by 7.9 eV laser light for Cu doped (a) Si_n (650 μJ/cm^2), (c) Sn_n (650 μJ/cm^2), (d) Pb_n (650 μJ/cm^2) clusters and (*) photoionized by 6.4 eV laser light for Cu doped (b) Ge_n (1 mJ/cm^2).

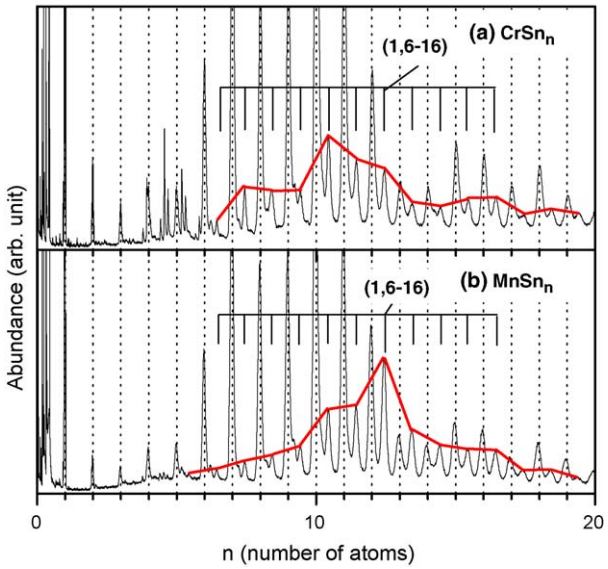

Fig. 3. Mass abundance spectra of (a) Cr doped Sn_n (650 μJ/cm^2) and (b) Mn doped Sn_n (650 μJ/cm^2) clusters radiated by 7.9 eV laser light.

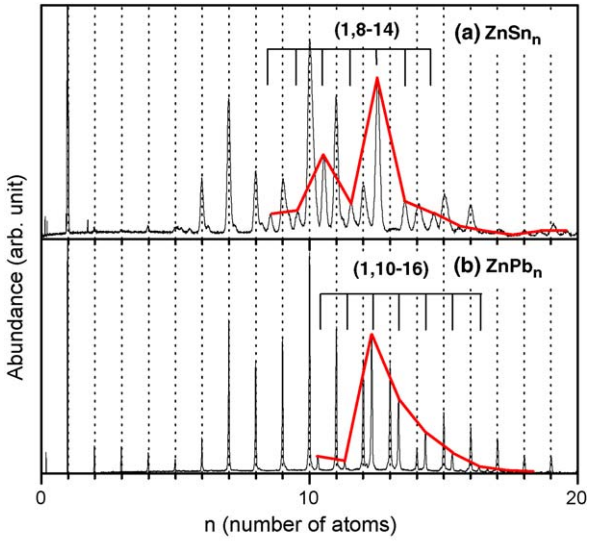

Fig. 5. Mass abundance spectra of Zn doped (a) Sn_n (97.5 μJ/cm^2) and (b) Pb_n (130 μJ/cm^2) clusters radiated by 7.9 eV laser light.

intermediate regime (0.1–0.5 mJ/cm^2) where it is often unclear, and strongly size dependent, whether the mass spectra reflect the abundance of either neutral or cationic species. In this regime, a curve of the ion yield as a function of the applied laser fluence, shows a quadratic (or higher order) behaviour, indicating two- (or multi-) photon ionization (without the irregular dependence characteristic for the combination of production and depletion in the fragmentation regime). In the latter case, species are denoted by $MS_n^{(+)}$. Related to this, it should be noted that nearly all species studied computationally in literature are in the neutral charge state.

Finally, some general remarks on the presented mass spectra are given. All mass spectra are presented as a function of the number of host atoms in the clusters (instead of the mass).

Vertical dotted lines are used to mark the pure S_n (S = Si, Ge, Sn, Pb) clusters. Peaks corresponding to singly doped species MS_n are connected by a solid line and the number of composing atoms is given as (1, n). Several spectra feature additional peaks that are not denoted or discussed in this paper and correspond to either oxidized or multiply doped species. The apparently worse mass resolution for Ge and Sn species compared to Si and Pb is partly due to their isotopical distribution over 5 amu (from 70 to 74 amu for the Ge atom and from 116 to 120 amu for Sn) versus 3 amu for the latter (from 28 to 30 amu for Si and from 206 to 208 for Pb). Moreover, the difference between the atomic mass of the dopants and lead is very large, while this is not the case for the other three host atoms. The atomic masses of Si, Ge, and Sn, respectively, are typically around half, in the order of, and double of the atomic mass of the dopants, which in all three cases leads to overlap between neighbouring mass peaks of pure and doped cluster species. The latter accounts for the seemingly better resolution of the doped lead cluster mass spectra compared to the other three cases.

3. Results

3.1. Cr doped group IVA clusters

A mass abundance spectrum of $CrSi_n^+$ photofragments after 6.4 eV laser irradiation at 0.9 mJ/cm^2 (Fig. 1a) shows significantly enhanced abundances for $CrSi_{15}^+$ and $CrSi_{16}^+$ in agreement with previous observations reported in ref. [1]. $CrSi_n^+$ (n = 14, 17, 18) clusters are observed less abundantly. The ionization energies of small Si_n clusters are higher than 6.4 eV and the abundance pattern is the result of fragmentation after multiphoton ionization. The peaks of lower mass clusters mainly correspond to pure Si_n^+, featuring the Si_{6-11}^+ photofragments in high abundance [30,39,40]. Pure Si_n and Ge_n clusters are known to undergo fission, instead of single atom evaporation, after high fluence laser irradiation and the Si_{6-11}^+ and Ge_{6-11}^+ species are the resulting daughter ions. The mass abundance spectrum for $CrGe_n^+$ photofragments (0.8 mJ/cm^2, Fig. 1b) well resembles the one for $CrSi_n^+$ species with relatively high abundances for $CrGe_n^+$ (n = 14–16). Cr doped Sn_n clusters after 6.4 eV laser irradiation (0.5 mJ/cm^2, Fig. 1c) are relatively abundant in the size range between n = 10 and 16 with slightly pronounced maxima for $CrSn_{15,16}^{(+)}$. Using 7.9 eV ionization (0.65 mJ/cm^2, Fig. 3a), a relatively enhanced abundance among the doped species is observed for $CrSn_{10}^+$ and, to a lesser extent, for $CrSn_{11}^+$ and $CrSn_{12}^+$. The above mentioned abundances were also observed at low fluences (not shown), indicating enhanced stabilities for neutral $CrSn_{15,16}$ and $CrSn_{10-12}$ clusters, respectively, using 6.4 and 7.9 eV photon energy. Contrary to the former three cases, no enhanced abundances are observed for $CrPb_{15,16}^+$ clusters while the spectrum (Fig. 3d) is marked by relatively high abundances for $CrPb_{10-12}^+$. Enhanced abundances are also observed for $CrPb_{10-12}$ neutrals, using 7.9 eV irradiation at low fluences.

3.2. Mn doped group IVA clusters

Stability patterns similar to Cr doped Si_n and Ge_n clusters are observed for the case of Mn doped $MnSi_n^+$ and $MnGe_n^+$ clusters (Fig. 2a and b). Besides $MnSi_{15}^{(+)}$ and $MnSi_{16}^{(+)}$, also $MnSi_{17}^{(+)}$ and $MnSi_{18}^{(+)}$ are observed relatively abundant. For germanium, doped species appear from $MnGe_{11}^{(+)}$ on, with (the sizes around) $MnGe_{15}^{(+)}$ showing relatively high abundances. For smaller sizes, pure Ge_n^+ clusters dominate the spectrum. Mn doped Sn_n clusters are much less abundantly observed compared to $CrSn_n$ species using 6.4 eV ionization. Distinct peaks can be identified corresponding to the sizes n = 13–16 with a sharp drop in abundance after $MnSn_{16}^{(+)}$ (Fig. 2c). Peaks corresponding to smaller sizes (n = 7–12) cannot be distinguished as they are too small and located in the broadened right flank of the very abundant pure $Sn_n^{(+)}$ clusters. However, using 7.9 eV ionization (0.6 mJ/cm^2, Fig. 3b), a strongly enhanced abundance of doped species is observed for $MnSn_{12}^+$ and, to a lesser extent, for $MnSn_{10}^+$ and $MnSn_{11}^+$. The same sizes are peculiarly abundant for very low fluences, i.e., neutral $MnSn_{12}$. Similarly, the spectrum probing the abundance of $MnPb_n$ species after 7.9 eV ionization (0.5 mJ/cm^2, Fig. 2d) features a strongly enhanced abundance corresponding to $MnPb_{12}^+$ (and $MnPb_{12}$ for very low fluences).

3.3. Cu doped group IVA clusters

The spectrum for $CuSi_n^+$ clusters after 7.9 eV laser irradiation (0.6 mJ/cm^2, Fig. 4a) shows a clearly different pattern compared to the former two dopants (Cr and Mn) featuring mainly $CuSi_6^+$, $CuSi_7^+$, and $CuSi_{10}^+$ as abundant sizes, while there is no sign for an enhanced abundance of doped $CuSi_n^+$ species in the size range n = 14–16. The situation is similar for $CuGe_n^+$ species showing enhanced abundances for $CuGe_7^+$ and $CuGe_{10}^+$ (6.4 eV, 1 mJ/cm^2, Fig. 4b). Cu doped Sn_n clusters are mainly detected in the size range between $CuSn_6^+$ and $CuSn_{16}^+$ with a strongly enhanced abundance for $CuSn_{10}^+$ (7.9 eV, 0.6 mJ/cm^2, Fig. 4c). Singly doped $CuPb_n^+$ clusters all are fairly abundant in the size range n = 10–14 with slightly pronounced abundance maxima for n = 10 and 12 (0.6 mJ/cm^2, Fig. 4d). Since Pb_{14}^+ exhibits a relative abundance minimum among pure Pb_n^+ clusters, the relatively high abundances of $CuPb_{13}^+$ and/or $CuPb_{14}^+$ are also remarkable. The abundance patterns for Cu doped Sn and Pb

clusters are very similar for very low fluences (7.9 eV), i.e., for the corresponding neutral species.

3.4. Zn doped group IVA clusters

Zn doped Si_n or Ge_n clusters turned out to be very difficult to produce. For singly doped species, only very low abundances of a limited number of sizes could be observed, not allowing us to draw any conclusions on peculiar abundance patterns. On the other hand, Zn doped Sn_n and Pb_n clusters are relatively easily produced. Mass spectra recorded using 7.9 eV post-ionization in the single photon ionization regime (0.1 mJ/cm^2, Fig. 5a and b) feature fairly enhanced abundances for $ZnSn_{10}$, $ZnSn_{12}$, and $ZnPb_{12}$. Again, as in the Cu doped case, the relatively high abundance of $ZnPb_{14}$ and $ZnPb_{13}$ compared to pure Pb_{14} is remarkable.

4. Discussion

4.1. Cr and Mn doped clusters

Table 1 summarizes the sizes that showed a peculiar abundance for the different dopant–host combinations studied. The mass spectrometric observation and stability of $CrSi_{15,16}^+$ species was presented in, to our knowledge, the first experimental study on binary or doped silicon clusters in 1987 by Beck [1]. However, as mentioned in Section 1, their structures remained basically undescribed until 2001. Both for $CrSi_{15}$ and $CrSi_{16}$, metal encapsulated Si_n cage structures account for their unusual stability [3]. An optimally close-packed structure obtained from a body-centered cubic unit has the lowest energy for $CrSi_{15}$, whereas for $CrSi_{16}$ the ground state is formed by an isomer with a capped fullerene-like cage. Although no computational results were found in literature for $MnSi_{15}$ and $MnSi_{16}$, their enhanced stabilities observed in our measurements are likely to relate to similar structures as for the case of Cr. Differently from MSi_n^+ (M = Cr, Mn) clusters, not only MGe_{15}^+ and MGe_{16}^+, but also MGe_{14}^+ is found to be relatively stable. Nevertheless, computationally, both $CrSi_{14}$ [17] and $CrGe_{14}$ [21] are predicted to have similar dopant-encapsulated decahedral ground state isomers. Experimentally, the (probably larger) Ge_{14} cage appears more favourable to host a Cr or Mn dopant compared to Si_{14}. For Mn doped Ge_{14} or Sn_{14} clusters, the perfect body-centered cubic isomer (with the dopant in the center) is suggested to be the lowest lying isomer [22]. The abundance patterns observed for MSn_n show a different picture depending on the applied photon energy for ionization. The mass abundance spectra, after ionization and fragmentation using 6.4 eV laser irradiation, feature similar stability patterns compared to MSi_n^+ and MGe_n^+. Enhanced stabilities for $CrSn_{15}^+$, $CrSn_{16}^+$, and $MnSn_{16}^+$ are likely to relate to the stable dopant-encapsulated structures that are already known for doped silicon and germanium clusters. The origin of the relative stability for $MnSn_{13}^+$, however, is less straightforward. Unfortunately, a recent computational study on doped MnS_n (S = Si, Ge, Sn, n = 8–12, 14) species [22], did not deal with this size. On the other hand, mass abundance spectra for MSn_n clusters after 7.9 eV ionization show enhanced abundances for $CrSn_{10}^{0,+}$ ($CrSn_{12}^{0,+}$ to a lesser extent) and $MnSn_{12}^{0,+}$, which may relate to highly symmetric close-packed D_{4h} and I_h structures, as were recently discussed for binary MPb_n and MSn_n clusters [22,25,26,28]. The appearance of enhanced abundances for different sizes (in the range from n = 10 to 16, depending on the details of the applied photon energy) may illustrate the transition which occurs in (doped) Sn_n clusters from covalently bound species for (doped) Si_n and Ge_n clusters, towards more metallic bonding (in Pb_n) [41]. The covalent (mixed sp^2/sp^3 type) bonding gives rise to (magic) cage-like structures (e.g., $MS_{15,16}$), different from the more compact (close-packed) structures for metal clusters (e.g., $MS_{10,12}$). As such, our results for Cr and Mn doped Sn_n seem to reflect the (size-dependent) competition between covalent and metallic bonding in doped Sn_n clusters.

It should be noted that the doped $MnSn_n$ data include the mass spectrometric observation of the enhanced abundance or stability for $MnSn_{12}$. As mentioned before, also at low 7.9 eV ionization fluences (<100 μJ/cm^2), in the single photon ionization regime, $MnSn_{12}$ is very abundantly detected. Recently, the latter was computationally predicted to form an icosahedral superatom with a high magnetic moment of 5μ_B [22]. Our results cannot reveal its magnetic properties but confirm its enhanced stability.

The enhanced abundances observed for $Cr/MnPb_{10,12}^{0,+}$ species most probably correspond to geometrically stable highly symmetric close-packed structures. Enhanced abundances for the same sizes were reported earlier for MPb_n^- (M = Ti, Cr, Mn, Fe, Co, Ni, Cu, Zn, Pd, Ag) anions [33].

4.2. Cu and Zn doped species

The enhanced stability for $CuSi_{10}^+$ confirms the observations by Beck [30]. Apart from $CuSi_{10}^+$, our experiments reveal enhanced abundances also for $CuGe_{10}^+$, $CuSn_{10}^{0,+}$, and $CuPb_{10}^{0,+}$. For Pb, $CuPb_{12}^{0,+}$ also can be added to this row. Among the Zn doped species, $ZnSn_{12}$, $ZnPb_{12}$, and, to a lesser extent, $ZnSn_{10}$ are detected very abundantly. $CuSi_n$ clusters (n = 4, 6, 8, 10, 12) are very thoroughly studied computationally [5,7,8]. An extensive isomer search for $CuSi_{10}$ claims that the high abundance observed in the mass spectra should not be ascribed to the geometric stability of a specific (highly symmetric) dopant-encapsulated structure, but rather to the existence of a multitude of near-degenerate isomers [7]. Important to note is that center-site structures for $CuSi_{10}$ are unfavourable. For the abundantly observed $CuGe_{10}^+$, $CuSn_{10}^{0,+}$, $CuPb_{10}^{0,+}$, and $CuPb_{12}^{0,+}$ structures, no computational information is available

Table 1
Summary of the peculiarly abundant sizes (n) for the 16 different MS_n (M = Cr, Mn, Cu, Zn, and S = Si, Ge, Sn, Pb) combinations studied

M	Si_n	Ge_n	Sn_n	Pb_n
Cr	$(15, 16)^+$	$(14, 15, 16)^+$	$(10–16)^+$, $(10)^0$	$(10, 12)^{+,0}$
Mn	$(15, 16)^{(+)}$	$(14, 15, 16)^{(+)}$	$(13, 16)^{(+)}$, $(12)^{0,+}$	$(12)^{+,0}$
Cu	$(10)^+$	$(7, 10)^+$	$(10)^{+,0}$	$(10, 12)^{+,0}$
Zn	–	–	$(10, 12)^0$	$(12)^0$

The charge state is indicated in the superscript.

in literature. Theoretical studies dealing wih MGe_n (M = Hf, W, Os, Ni, Zn, n = 10, 12), MS_n (M = Be, Zn, Cd, Mg, and S = Si, Ge, Sn, n = 8–12, 14), and MS_{10} (M = Ni, Pd, Pt, and S = Si, Ge, Sn, Pb) [22,24,25] lead to endohedral ground state structures for most of the investigated species. However, the stability and exact symmetry of the different systems is 'case' dependent and can be tailored by suitably choosing dopant and host.

Nevertheless, the enhanced stabilities observed for $ZnSn_{10}$, $ZnSn_{12}$, $ZnPb_{12}$, $CuSn_{10}{}^{0,+}$, $CuPb_{10}{}^{0,+}$, and $CuPb_{12}{}^{0,+}$ probably relate to highly symmetric dopant-encapsulated D_{4d} (bicapped square antiprism) and I_h (icosahedron) structures for the 11 and 13 atom species, respectively. After all, the D_{4d} structure is found to be the ground state structure for all computed MSn_{10} and MPb_{10} structures in literature, i.e., $BeSn_{10}$ [22], Ni/Pd/Pt//Sn/Pb_{10} [25], $AlPb_{10}{}^+$ [26], and $NiPb_{10}{}^{2-}$ [29], and the I_h structure is the lowest energy isomer for all known MSn/Pb_{12} structures, i.e., $AlPb_{12}{}^+$ [26], MSn_{12} (M = Be, Mg, Ca, Mn, Zn, Cd) [22], $PtPb_{12}{}^{2-}$ [28]. Finally, contrary to the observation of $MnSn_{12}$, the computationally predicted special stability of $ZnGe_{12}$ as a metal-encapsulated icosahedral superatom [20,24] is not confirmed by our measurements. The results mentioned above seem to confirm that the possibility of d-band filling of the dopant atom with the dangling bond electrons from the Si_n and Ge_n cages is crucial in obtaining stable dopant-encapsulated structures [24,37]. Apparently, contrary to Cr and Mn, the complete occupation of the Zn and Cu 3d orbitals prevents the formation of highly symmetric dopant-encapsulated Zn or Cu doped Si_n and Ge_n clusters.

5. Conclusion

Besides the confirmation of the previously observed special stability of a number of endohedral doped silicon clusters, our experiments provide the first experimental observation of a number of very abundantly produced species among its doped heavier group IVA congeners: germanium, tin, and lead. As such, our measurements partly cover the large variety of metal dopant—group IVA host combinations that have been accessed theoretically in literature. The sizes showing enhanced abundance are summarized in Table 1 and, apart from Cu doped Si_n or Ge_n, are likely to relate to endohedral structures: irregular cages for the doped Si_n and Ge_n species, highly symmetric close-packed structures for the doped Pb_n clusters. The doped Sn_n species seem to cover the transition between covalently bound endohedral silicon and germanium cages and metallically bound lead clusters. Several of the abundantly observed sizes were computed previously in literature. While the special stability of $ZnGe_{12}$ was not detected, our experiments confirm the enhanced stability of the metal doped magic magnetic superatom $MnSn_{12}$.

Acknowledgements

This work is supported by the Fund for Scientific Research—Flanders (FWO), the Flemish Concerted Action (GOA/2004/02), and the Belgian Interuniversity Poles of Attraction program (IAP/P5/01). S.N. and E.J. are Postdoctoral Researchers of the FWO.

References

[1] S.M. Beck, J. Chem. Phys. 87 (1987) 4233.
[2] R.B. King, Z. Phys. D 18 (1991) 189.
[3] V. Kumar, Y. Kawazoe, Phys. Rev. B 65 (2002) 073404.
[4] K. Jackson, B. Nellermoe, Chem. Phys. Lett. 254 (1996) 249.
[5] F. Hagelberg, I. Yanov, J. Leszczynski, J. Mol. Struct. 487 (1999) 183.
[6] V. Kumar, Y. Kawazoe, Phys. Rev. Lett. 87 (2001) 045503.
[7] C. Xiao, F. Hagelberg, W.A. Lester, Phys. Rev. B 66 (2002) 075425.
[8] F. Hagelberg, C. Xiao, W.A. Lester, Phys. Rev. B 67 (2003) 035426.
[9] P. Sen, L. Mitas, Phys. Rev. B 68 (2003) 155404.
[10] T. Miyazaki, H. Hiura, T. Kanayama, Phys. Rev. B 66 (2002) 121403.
[11] V. Kumar, C. Majumder, Y. Kawazoe, Chem. Phys. Lett. 363 (2002) 319.
[12] S.N. Khanna, B.K. Rao, P. Jena, Phys. Rev. Lett. 89 (2002) 016803.
[13] J. Lu, S. Nagase, Phys. Rev. Lett. 90 (2003) 115506.
[14] V. Kumar, T.M. Briere, Y. Kawazoe, Phys. Rev. B 68 (2003) 155412.
[15] V. Kumar, Comp. Mater. Sci. 30 (2004) 260.
[16] C. Majumder, S.K. Kulshreshtha, Phys. Rev. B (2004) 245426.
[17] H. Kawamura, V. Kumar, Y. Kawazoe, Phys. Rev. B 70 (2004) 245433.
[18] H. Kawamura, V. Kumar, Y. Kawazoe, Phys. Rev. B 71 (2005) 075423.
[19] A.K. Singh, V. Kumar, Y. Kawazoe, Phys. Rev. B 71 (2005) 115429.
[20] V. Kumar, Y. Kawazoe, Appl. Phys. Lett. 80 (2002) 859.
[21] V. Kumar, Y. Kawazoe, Phys. Rev. Lett. 88 (2002) 235504.
[22] V. Kumar, Y. Kawazoe, Appl. Phys. Lett. 83 (2003) 2677.
[23] V. Kumar, Eur. Phys. J. D 24 (2003) 227.
[24] J. Lu, S. Nagase, Chem. Phys. Lett. 372 (2003) 394.
[25] V. Kumar, A.K. Singh, Y. Kawazoe, Nano Lett. 4 (2004) 677.
[26] S. Neukermans, E. Janssens, Z.F. Chen, R.E. Silverans, P.V.R. Schleyer, P. Lievens, Phys. Rev. Lett. 92 (2004) 163401.
[27] X. Zhang, G. Li, X. Xing, X. Zhao, Z. Tang, Z. Gao, Rapid Commun. Mass Spectrom. 15 (2001) 2399.
[28] E.N. Esenturk, J. Fettinger, Y.F. Lam, B. Eichhorn, Angew. Chem. Int. Ed. 43 (2004) 2132.
[29] E.N. Esenturk, J. Fettinger, B. Eichhorn, Chem. Comm. (2005) 247.
[30] S.M. Beck, J. Chem. Phys. 90 (1989) 6306.
[31] H. Hiura, T. Miyazaki, T. Kanayama, Phys. Rev. Lett. 86 (2001) 1733.
[32] M. Ohara, K. Koyasu, A. Nakajima, K. Kaya, Chem. Phys. Lett. 371 (2003) 490.
[33] X. Zhang, Z. Tang, Z. Gao, Rapid Commun. Mass Spectrom. 17 (2003) 621.
[34] W. Zheng, J.M. Nilles, D. Radisic, K.H. Bowen Jr., Chem. Phys. 122 (2005) 071101.
[35] K. Koyasu, M. Akutsu, M. Mitsui, A. Nakajima, J. Am. Chem. Soc. 127 (2005) 4998.
[36] H.W. Kroto, J.R. Heath, S.C. O'Brien, R.F. Curl, R.E. Smalley, Nature 318 (1985) 582.
[37] G. Mpourmpakis, G.E. Froudakis, A.N. Andreotis, M. Menon, J. Chem. Phys. 119 (2003) 7498.
[38] W. Bouwen, P. Thoen, F. Vanhoutte, S. Bouckaert, F. Despa, H. Weidele, R.E. Silverans, P. Lievens, Rev. Sci. Instrum. 71 (2000) 54.
[39] J.R. Heath, Y. Liu, S.C. O'Brien, Q.L. Zhang, R.F. Curl, F.K. Tittel, R.E. Smalley, J. Chem. Phys. 83 (1985) 5520.
[40] Q.L. Zhang, Y. Liu, R.F. Curl, F.K. Tittel, R.E. Smalley, J. Chem. Phys. 88 (1987) 1670.
[41] A.A. Shvartsburg, M.F. Jarrold, Chem. Phys. Lett. 317 (2000) 615.